Journal of Materials Chemistry C

Accepted Manuscript

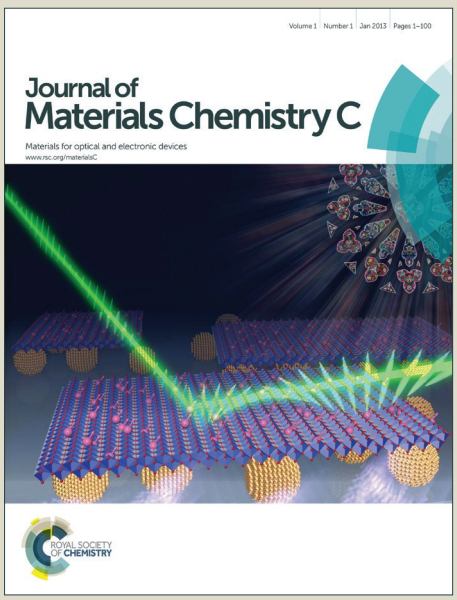

ROYAL SOCIETY OF CHEMISTRY

www.rsc.org/materialsC

Journal Name

ARTICLE

Initial Hydrogen-Bonding Dynamics of Photoexcited Coumarin in Solution with Femtosecond Stimulated Raman Spectroscopy

Fangyuan Han,‡[a,b] Weimin Liu,‡[a] Liangdong Zhu,[a,c] Yanli Wang[a] and Chong Fang*[a,c]

Received 00th March 20xx,
Accepted 00th March 20xx

DOI: 10.1039/x0xx00000x

www.rsc.org/

Hydrogen bond (H-bond) making and breaking dynamics in solute-solvent systems represent a fundamental class of intermolecular interactions that play a crucial role in numerous chemical reactions and biological processes. To reveal the initial H-bond dynamics following electronic excitation of a shape-responsive fluorophore in condensed phase, we develop tunable femtosecond stimulated Raman spectroscopy (FSRS) with 660/670–760 nm Raman pump/probe pulses to pre-resonantly enhance transient Coumarin 102 (C102) species in the singly excited state S_1 following 400 nm photoexcitation. Within 400 fs (<140 fs time constant), prominent vibrational marker bands at ~1700 and 1740 cm^{-1} of the photoexcited fluorophore exhibit an ultrafast decay and rise, respectively, revealing that the H-bond cleaves on that timescale. The subsequent dynamics of the 1740 cm^{-1} mode intensity show ~13 ps rise, 37 ps and >1 ns decay, which are attributed to solvation of the nascent free C102, H-bond reformation of the solvated C102, and radiative emission from the relaxed excited state. The mechanistic understanding is corroborated by the time-resolved excited-state absorption of C102 in ethanol as a function of probe wavelength in the visible to near-IR range, as well as ground-state bleaching signal evolution in the UV region. The direct observation of H-bond breaking events followed by excited-state population bifurcation and solvation of both free and H-bonded C102 in ethanol provides an unambiguous, rich portrait of structural dynamics of a fluorophore in solution on crucial molecular timescales (fs to ps). These insights will enable the rational development of photosensitive molecules in general with prescribed functions for materials and biological applications.

Introduction

Hydrogen (H)-bonding has been a constant research interest due to its crucial functional role in numerous chemical and biological systems from organic chromophores to enzyme proteins.[1-5] Despite extensive efforts to achieve better understanding of this fundamental site-specific intermolecular or intramolecular interaction in various environments, the detailed picture of H-bond making and breaking remains far from complete.[3,6] To date, most research on H-bonding dynamics has focused on the electronic ground state, while much less is known about electronic excited states and local solute-solvent interactions.[7,8] This limitation hinders our mechanistic understanding of the underlying photophysics and photochemistry, which power molecular functions ranging from bioluminescence to light harvesting.[5,9-11] Therefore, structural dynamics insights on the intrinsic timescales are required to enable the rational design and improvement of molecular fluorophores and other photosensitive materials in general for the broad science and engineering community.

The challenge to unravel excited-state H-bonding dynamics (ESHBD) is rooted in the complexity of excited-state potential energy landscape that comprises coupled electron and nuclear motions, which are transient, multidimensional, and difficult to characterize from either experimental or theoretical perspectives. In many systems, ESHBD occurs on a sub-picosecond (sub-ps) to ps timescale with electronic redistribution and site-specific structural rearrangements.[3,7] Structural techniques including diffraction methods and NMR spectroscopy either cannot reach, or are still under development to achieve higher time resolution.[12] In contrast, ultrafast electronic spectroscopy such as femtosecond (fs) fluorescence up-conversion and transient absorption can probe population dynamics in electronic excited states with fs time resolution, but are intrinsically insensitive to vibrational motions that directly report on the making/breaking or strengthening/weakening of H-bonds at molecular sites, or anharmonic coupling between vibrational modes that determines energy flow and dissipation.[13,14] This "local" sensitivity is an inherent staple of vibrational spectroscopy, and the excellent resolving power has enabled its fs version to

[a] Oregon State University, Department of Chemistry, 263 Linus Pauling Science Center (lab), 153 Gilbert Hall (office), Corvallis, OR 97331, USA. *E-mail: Chong.Fang@oregonstate.edu; Fax: +1 541 737 2062; Tel: +1 541 737 6704
[b] Current address: Guangxi Power Grid Electric Power Research Institute, Nanning, Guangxi 530023, China
[c] Oregon State University, Department of Physics, 301 Weniger Hall, Corvallis, OR 97331, USA

† Electronic Supplementary Information (ESI) available: Additional Fig. S1—S4 followed by additional discussions on schematic of the tunable FSRS setup, steady-state electronic spectroscopy of C102 in various solvents, femtosecond transient absorption of C102 in ethanol, and time-resolved 400/400 nm pump-probe data of C102 in ethanol, and references. See DOI: 10.1039/x0xx00000x

‡ These authors contribute equally to this work.

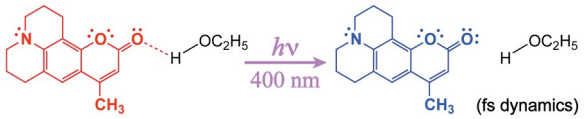

Scheme 1 The H-bond between the carbonyl oxygen of C102 (solute) and the hydrogen of the hydroxyl group of ethanol (solvent) cleaves on the femtosecond timescale upon UV (400 nm) excitation.

be actively developed as a table-top apparatus to study molecular systems during the past several decades.[3,4,15,16]

Hitherto, one of the most successful experimental methods to study ESHBD has been optical pump/mid-IR probe spectroscopy, which records time-resolved vibrational spectra with a time resolution of ~200 fs.[17] Using this technique, Nibbering and co-workers observed an ultrafast blueshift of the C=O stretching band of Coumarin 102 (C102), a widely used fluorescent dye and paradigm for microviscosity and solvatochromic studies, upon electronic excitation when H-donors such as chloroform ($CHCl_3$) and phenol are present.[18-20] The parent family, 7-aminocoumarins as laser dyes, display tunable photophysical properties, excellent photostability, and high fluorescence quantum yield in many common solvents.[21] In general, coumarin refers to a large class of compounds that include fused benzene and α-pyrone rings. More than 1,300 different coumarin compounds have been found from natural sources such as fungi and bacteria and especially green plants. Besides applications as fluorescent probes, pathological ion probes and biological stains, coumarin derivatives have been reported to be pharmacologically important because of their anticoagulant, antioxidative, anti-inflammatory, analgesic, anti-neurodegenerative, anticancer, and anti-mutagenic properties.[22] It has been proposed that weak interactions such as van der Waals force and H-bonding between active sites of organisms and certain atomic sites of coumarin could play a crucial role in their key performance metrics. To date, a thorough understanding of such interactions, even for simple systems like C102 in H-donating solvents, remains lacking. Therefore, it is of fundamental importance in studying these intermolecular interactions. Furthermore, the rational design strategies can be greatly facilitated by understanding the structure-property relationships and action mechanisms of those coumarin-derived systems particularly in solution.

Notably, the carbonyl group in C102 is the only site that is responsible for both H-bond formation and electron acceptance,[23] given that the degrees of freedom commonly found in 7-aminocoumarins are greatly reduced by structural constraints in the C102 framework (Scheme 1). Within 200 fs after ~400 nm photoexcitation, the C=O stretching band blueshifts by ~40 cm^{-1} compared to the ground state (S_0), toward a peak frequency that matches the C=O stretching mode of C102 in the nonpolar, aprotic solvent such as tetrachloroethylene (C_2Cl_4). It was concluded that the H-bond between C102 and the H-donor cleaves on this ultrafast timescale.[18,19] Theoretical work on ESHBD of C102 in different solutions, however, shows a possibility of the H-bond strengthening rather than cleavage upon UV excitation. Using density functional theory (DFT)/time-dependent DFT (TDDFT) methods[24] for electronic ground/excited state calculations, Zhao and Han noticed a decrease in the length of the H-bond C=O···H–O in the C102-phenol complex upon the $S_0 \rightarrow S_2$ electronic transition induced by 400 nm photoexcitation, accompanied by the lengthening of both C=O (on the C102 side, H-acceptor) and H–O (phenol side, H-donor) bonds.[25] Furthermore, the calculated H-bond binding energy was found to be substantially higher in the initial excited state than in S_0, indicating that a H-bonded complex is more energetically favorable than a free C102 molecule.

The discrepancy between experimental and theoretical results largely arises from the typical inaccessibility of potential energy surface (PES) geometry within and near the Franck-Condon (FC) region, which governs the evolution of non-stationary excited-state wavepackets at early time. The optical pump/mid-IR probe technique is known to exhibit unwanted coherence effects that seriously mask the dynamics of interest in the first few hundred femtoseconds (fs), the time region in which critical conformational dynamics could occur. On the other hand, it is computationally challenging and currently unfeasible to fully characterize the FC region other than the equilibrium/stationary configuration either in the electronic ground or excited state. With recent nonlinear spectroscopic advances in our lab,[11,26-28] we revisited this foundational topic and experimentally examined the ESHBD of C102 molecules in ethanol using femtosecond transient absorption and femtosecond stimulated Raman spectroscopy (FSRS), with an emphasis on the first few hundred fs following 400 nm photoexcitation. Our goal is to provide unambiguous and deeper insights into this crucial time regime that holds the key to elucidating the photochemical reaction coordinate of a fluorophore in solution starting from time zero.

Results and discussion

Femtosecond transient absorption

Two main electronic features have been identified by Morlet-Savary et al. in transient spectra of C102 in alcoholic solvents.[29] In 1-propanol, a strong stimulated emission band is present between 420 and 550 nm, and a weak, broad excited state absorption (ESA, $S_1 \rightarrow S_n$) band extends into the near-IR range. Limited by their ps-laser pump-probe setup, the dynamics was typically plotted after ~35 ps with a time resolution of ~10 ps. In comparison, our transient absorption data (see Fig. S3, ESI†) capture the temporal evolution of the ESA band from –1.5 to 600 ps over the spectral range of 625–725 nm. The kinetic traces at different probe wavelengths are least-squares fitted with multiple exponentials convoluted with the ~140 fs instrument cross-correlation function (see Experimental),[30] and the detailed fitting results are listed in Table 1.

As shown in Fig. 1, the observed decay components exhibit clear dependence on the probe wavelengths. Similar to kinetic traces obtained from optical pump/mid-IR probe experiment, a spike-like feature appears near time zero (Fig. 1c insert) due

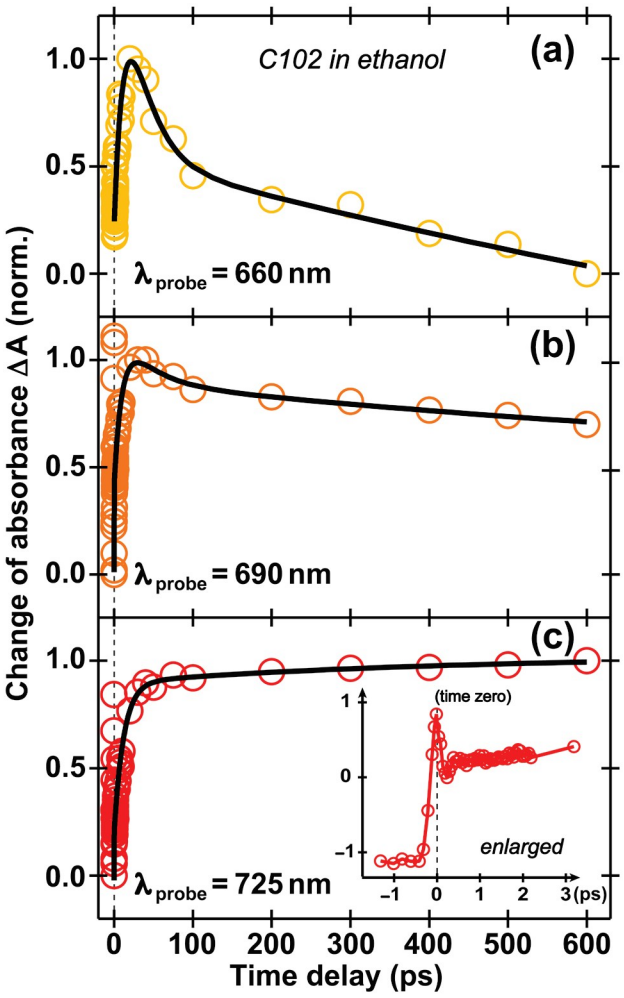

Fig. 1 Wavelength-dependent transient absorption of C102 in ethanol up to 600 ps following 400 nm photoexcitation with the probe wavelength at (a) 660, (b) 690, and (c) 725 nm. The least-squares fits (black solid curve) are superimposed on the experimental data points (dark yellow, orange, and red hollow circles, respectively to represent the reddening of the probe pulse). The enlarged early-time dynamics around photoexcitation time zero is shown in (c) insert.

to coherent effects, masking the solute dynamics in the first few femtoseconds after 400 nm photoexcitation. This artifact diminishes at long probe wavelengths (>670 nm) with indication of an ultrafast rising component (<140 fs, t_1 in Table 1). This initial rise with a characteristic lifetime shorter than 140 fs is consistent with the fastest dynamic process revealed by the previous optical pump/mid-IR probe technique, which was interpreted as a signature of H-bond cleavage after photoexcitation around 400 nm.[18] A second rise component (~10 ps time constant, t_2 in Table 1) exists at all probe wavelengths across our detection spectral window. At probe wavelengths <700 nm, two decay components with ps and ns time constants (t_3 and t_4) are retrieved from the least-squares fitting. As the probe shifts further to the red, the first decay component (t_3) shows an increase of the time constant with a concomitant weight decrease, indicative of the overlapping transient electronic features. Because our experimental time window is up to ~600 ps due to the 10 cm translation stage we use, the exact number of the nanosecond (ns) time constant (t_4) is not precisely determined and reported. Based on these transient absorption results, we strategically tune the Raman pump to 660 nm (Fig. S1, ESI†) to take advantage of resonance enhancement because the Raman pump wavelength is now close to the excited-state absorption peak of C102.

Time-resolved excited-state FSRS studies

To gain structural dynamics insights and mechanistic understanding of ESHBD for a shape-responsive fluorophore in solution, time-resolved vibrational spectroscopy provides the essential atomic choreography at the chemical bond level on intrinsic molecular timescales.[5,11] Figure 2 presents the time-resolved excited-state FSRS spectra of C102 in ethanol. An array of vibrational peaks are prominent in the high-frequency region (>1500 cm^{-1}), with two marker bands at ~1700 and 1740 cm^{-1} (the chromophore C=O stretching motion) being especially pertinent to the H-bonding dynamics of primary interest. When compared with ground-state FSRS spectra of C102 in ethanol (CH_3CH_2OH, protic and H-donating) and tetrachloroethylene ($Cl_2C=CCl_2$, aprotic and non-H-donating) as shown in Fig. 2 left-top panel, it is clear that the 1700 and 1740 cm^{-1} modes correspond to the H-bonded and non-H-bonded C=O stretching motion, respectively.

There is also indication of excited-state band splitting (see Fig. 2 right panel, the enlarged spectra between 1670—1800

Probe wavelength (nm)	t_1 (fs) [a]	t_2 (ps)	t_3 (ps)	t_4 (ns)
630	-	(+) 13.7	(–) 19.3 (69%)	(–) >1 (31%)
660	-	(+) 13.2	(–) 26.4 (53%)	(–) >1 (47%)
690	(+) <140	(+) 10.2	(–) 36.8 (40%)	(–) >1 (60%)
700	(+) <140	(+) 10.0	(–) 42.5 (37%)	(–) >1 (63%)
710	(+) <140	(+) 9.9	(–)	(–)
725	(+) <140	(+) 12.1	(+) 380	(–)

Table 1 Best-fit dynamic parameters at representative probe wavelengths in transient absorption following 400 nm photoexcitation.

[a] In all cases, (+) represents a rising component, (–) represents a decay component, and the numbers in parentheses represent the relative amplitude weights of the corresponding decay components from least-squares fitting of the time-resolved experimental data trace.

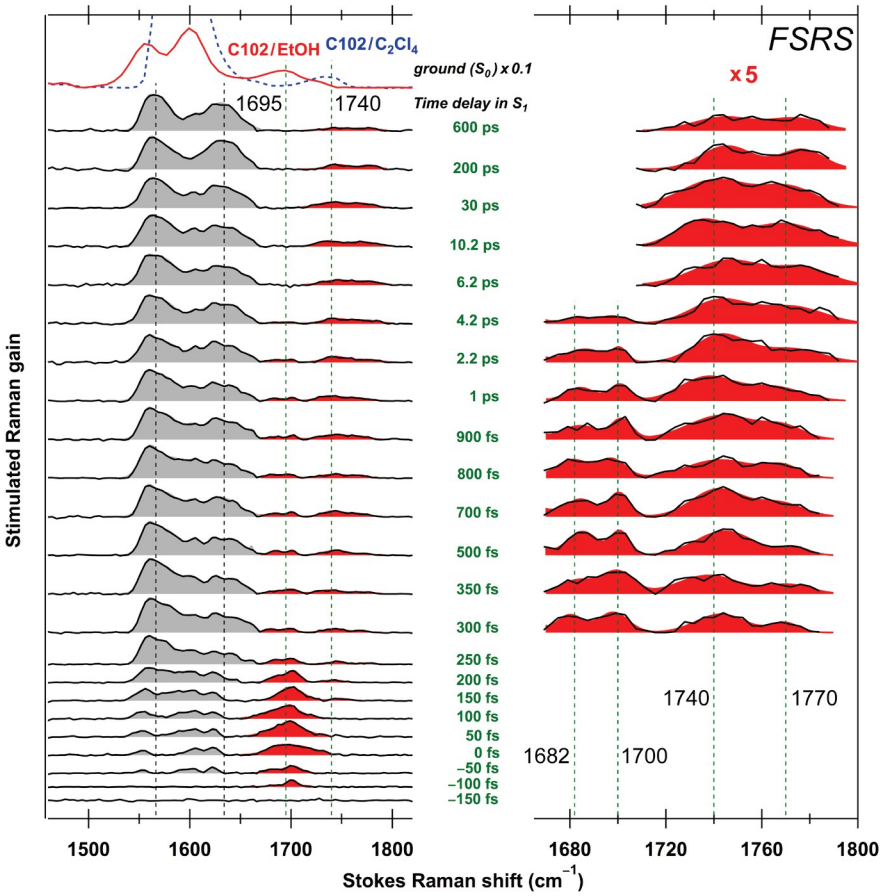

Fig. 2 Time-resolved excited-state FSRS data of C102 dye molecules in ethanol up to 600 ps following 400 nm photoexcitation between ca. 1450—1800 cm^{-1}. The corresponding time delay (green label) is noted beside each spectrum (black solid lines). The enlarged (×5) region between 1670—1800 cm^{-1} is shown on the right with the red shades (multi-gaussian peak fits) highlighting the small but statistically significant C=O stretching signals in S_1. The scaled ground-state spectra of C102 dissolved in ethanol (red solid) and C_2Cl_4 (blue dashed) are shown at the top of the left panel with the latter trace truncated at the main peak to highlight the weak C=O stretch feature. Vibrational marker bands are highlighted by vertical green dashed lines with center frequencies noted in the C=O stretch region. Two prominent Raman bands (gray shades) below 1670 cm^{-1} are marked by black dashed lines at 1567 and 1634 cm^{-1}, respectively, which consist of a number of overlapping vibrational modes mainly associated with the chromophore ring modes (e.g., C=C stretch, phenyl and lactone ring deformation from our Gaussian DFT calculations).[24]

cm^{-1}). This is consistent with the excited-state IR spectra reported in previous publications that showed an asymmetric lineshape of the C=O stretching band, whose origin has not been unambiguously identified.[18,19] We suspect that the main origin for this broad band splitting is inhomogeneity in solution which may involve different charge-transfer type of interactions between photoexcited C102 and surrounding solvent (*e.g.*, ethanol) molecules. Moreover, the direct observation of the split bands evolving in S_1 provides useful insights about the adjacent mode assignment. For example, the 1682 cm^{-1} mode represents a further redshift to the 1700 cm^{-1} mode that matches the H-bonded C=O stretch of C102 in ethanol, while the lower-frequency mode rises slower than the higher-frequency mode within ~4 ps (see Fig. 2, right). This indicates that the 1682 cm^{-1} mode may involve a transient C102 population that experiences H-bond strengthening in the excited state on the fs to ps timescale (i.e., non-stationary dynamics in and near the FC region before reaching the equilibrium state). On the other hand, the 1770 cm^{-1} mode is further blueshifted than the 1740 cm^{-1} mode that matches the non-H-bonded C=O stretch of C102 in C_2Cl_4, while the higher-frequency mode rises slower than the lower-frequency mode within ~100 ps (Fig. 2 right) followed by the intensity decay on longer timescales. This suggests that the 1770 cm^{-1} mode involves a transient C102 population that experiences further H-bond breaking in the excited state on the ps timescale, which occurs much later than the aforementioned 1682 and 1700 cm^{-1} modes. Based on the peak intensity and overall dynamic pattern, we find that the dominant structural change of photoexcited C102 in ethanol is the H-bond breaking at the C=O site on the initial fs to ps timescale. Notably, these fine details about transient vibrational mode frequency shift and intensity dynamics are enabled by our tunable FSRS technique that greatly increases the signal-to-noise ratio of excited-state C102 Raman features. We can thus gain insights into structural dynamics pertaining to H-bonding interactions, including those fleeting and peripatetic configurations that are responsible for the rise and decay of C=O stretching bands observed herein.

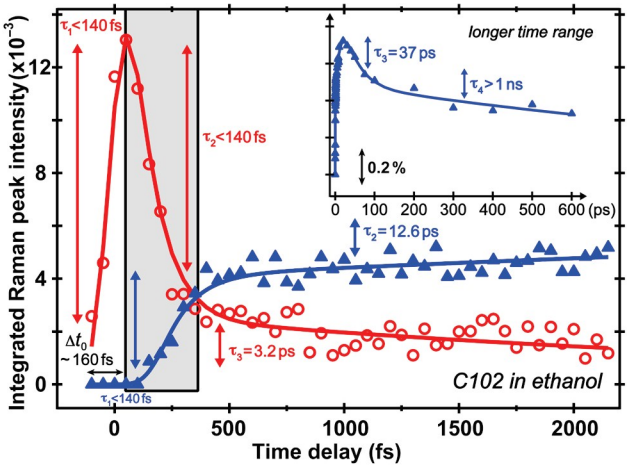

Fig. 3 Kinetic intensity plot of the excited-state Raman modes of C102 in ethanol from the time-resolved FSRS data shown in Fig. 2. The H-bonded species (~1700 cm^{-1} band, red) and non-H-bonded species (~1740 cm^{-1} band, blue) show contrasting temporal evolution. The least-squares fits (solid curves) are overlaid with the data points (red hollow circles or blue filled triangles) up to 2.2 ps with the fitted time constants labeled near the corresponding kinetic phase. The overall dynamics of the 1740 cm^{-1} band up to 600 ps following 400 nm photoexcitation and the associated longer decay time constants are shown in the insert. The gray shade highlights the crucial H-bonding dynamics region within 500 fs of the 400 nm photoexcitation.

Kinetic intensity analysis of vibrational marker bands

Detailed quantitative analysis of the total integrated Raman peak intensity (1682/1700 cm^{-1} modes are collectively referred to as the ~1700 cm^{-1} mode, and 1740/1770 cm^{-1} modes are collectively referred to as the ~1740 cm^{-1} mode) shows distinct dynamics for the two excited-state vibrational marker bands (Fig. 3). The overlap between these adjacent, broad spectral bands attributed to the same free/H-bonding population prevents us from precise analysis of individual mode dynamics, but their integrated intensity should reflect the overall H-bonding configuration change at the carbonyl end of C102 within our detection time window. Firstly, the kinetic trace of the 1700 cm^{-1} mode rises (with <140 fs time constant) ~160 fs earlier than the 1740 cm^{-1} mode. Secondly, the subsequent ultrafast drop (fitted time constant <140 fs) of the 1700 cm^{-1} mode intensity is accompanied by a concomitant rise of the 1740 cm^{-1} mode intensity (with <140 fs time constant, Fig. 3, shaded gray area). Thirdly, the 1700 cm^{-1} mode diminishes rapidly with 3.2±1.0 ps time constant and becomes unidentifiable ~6 ps after photoexcitation, while the 1740 cm^{-1} mode shows additional dynamics on a much longer timescale. In particular, the second rise time constant is 12.6 ± 3.3 ps, and the 1740 cm^{-1} band area reaches its maximum ~20 ps after excitation, followed by decay with 37 ± 10 ps (58% weight) and > 1 ns (42% weight) characteristic time constants, respectively.

In each kinetic trace, all the fitted components share the same starting time t_0 that is assuming the simultaneous excitation of these adjacent vibrational modes.[30,31] In that context, the fitted time zero of the 1740 cm^{-1} kinetic trace is 160 ± 50 fs (Δt_0 in Fig. 3) "behind" the time zero of the 1700 cm^{-1} kinetic trace. Since the 1740 cm^{-1} band is a marker band of free C102, it can be concluded that a portion of excited-state C102 molecules undergoes H-bond cleavage within 160 ± 50 fs after 400 nm excitation. In contrast, the directly excited free C102 molecules, i.e. the non-H-bonded ground-state C102 excited by the 400 nm excitation pulse, should not make a large contribution to the 1740 cm^{-1} band. This is because the efficiency of 400 nm excitation is very low for free C102 molecules (see Fig. S2, ESI†). Furthermore, if the directly excited free C102 molecules were an important origin of the 1740 cm^{-1} band in excited-state FSRS spectra, we would have observed a simultaneous rise of both ~1700 and 1740 cm^{-1} bands. Notably, our data also eliminate the possibility of H-bond cleavage as the only pathway of excited-state dynamics, wherein the 1700 cm^{-1} band should vanish immediately when the 1740 cm^{-1} band appears. In other words, the H-bonds are ruptured only in a portion of, but not all photoexcited C102 molecules. This type of information can only be retrieved from the simultaneous observation and analysis of reactant and product species during a chemical reaction, which in this case involves an ultrafast H-bond breaking event.

The early-time structural dynamics is clearly resolved by FSRS for the first time, providing us with critical information of the excited-state PES near the FC region. The delayed rise of the 1740 cm^{-1} band is a strong evidence that an excited-state population of non-H-bonded C102 is generated after ~160 fs following 400 nm photoexcitation. Moreover, this increase in the excited-state non-H-bonded C102 population is accompanied by the decrease of the H-bonded C102 population, evinced by the concomitant drop in the 1700 cm^{-1} mode intensity pertaining to the same C=O bond (Fig. 3 gray shade), indicative of causality. It is therefore confirmed that (1) the fluorophore-solvent H-bond C=O···H cleaves upon 400 nm photoexcitation, and (2) this cleavage occurs in the original excited state S_1 rather than during electronic excitation. The first point has been reported using optical pump/mid-IR probe technique,[18,23,32] but it should be noted that the technique was unable to distinguish whether the H-bond ruptures during or after photoexcitation due to strong coherent artifacts including perturbed free induction decay near time zero (see Fig. 1c insert for example).[23] Using the two-pulse photon echo technique, Nibbering and co-workers deduced that an electronic hopping event, which is possibly but not necessarily the H-bond cleavage, occurs ~180 fs after photoexcitation of C102 in H-donating solvents.[32] To our best knowledge, the current work is the first time that this case has been clarified with direct spectral evidence based on FSRS vibrational dynamics in S_1 starting from time zero of photoexcitation.

Notably, we focus on the two C=O stretching modes here because they are spectrally separated from other strong vibrational modes below 1670 cm^{-1}, and they directly report on the local H-bond making and breaking events with high frequency sensitivity, in addition to the high temporal resolution afforded by the FSRS technique. The other Raman modes can also be analyzed to yield time constants. However, due to spectral overlap between those more delocalized ring modes below 1670 cm^{-1} (see Fig. 2, and Experimental) it is not

straightforward to deduce unambiguous mechanistic insights. We remark that systematic modification of the molecular framework by adding specific functional groups may be a useful strategy to unravel the detailed choreography of the fluorophore ring system during H-bond breaking and making events as discussed extensively above.

Mechanistic understanding of H-bond dynamics

The comparison between the S_1 vibrational mode intensity evolution from FSRS and femtosecond transient absorption signal brings deeper insights into the geometries of PES and excited-state dynamics of solvated C102 molecules. In particular, the dynamics of the non-H-bonded C=O stretching mode (1740 cm^{-1}, Fig. 3 insert) probed by FSRS is similar to the dynamics revealed by transient absorption at shorter probe wavelengths, *e.g.*, 690 nm (see Table 1). This result suggests that (1) the 1740 cm^{-1} Raman mode intensity change largely reflects the excited-state population change, rather than a change in Raman polarizability or resonance conditions,[16] of non-H-bonded C102, and (2) it is the excited-state population dynamics of non-H-bonded C102 rather than H-bonded C102 that is being probed at shorter wavelengths in transient absorption. The apparent dependence of the observed dynamics on probe wavelength (Fig. 1 and Table 1) likely arises from the overlap between electronic features of H-bonded and non-H-bonded C102, wherein the former (latter) species contributes a transient absorption band at the red (blue) side of ~710 nm (see Fig. S3d, ESI†). This result suggests that the H-bonded species re-accumulates on the hundreds of ps timescale due to the surrounding solvent reorganization, and exhibits an ESA feature that grows (Fig. 1c) while the non-H-bonded species decreases with time (Fig. 1a-b). Ideally, the time-resolved transient spectra can be analyzed using methods such as global and target analysis to separate the dynamics of each species.[33] The strategy is challenging to implement in this work due to truncation of the broad excited state absorption band at both ends of our spectral window, as well as a lack of pre-knowledge of the actual electronic band shape.

The ~10 ps rising component exists at all probe wavelengths (Table 1) and is consistent with the reported longitudinal relaxation time of ethanol.[29,34,35] We attribute this component to the solvation of excited-state non-H-bonded C102 emerging via ultrafast H-bond cleavage. This time constant closely matches the slower solvation timescale for C102 in neat aniline (~7 ps) that represents a diffusive restructuring of the solvation shell.[23] Steady-state and time-resolved fluorescence study of C102 in H-donating environments by Liu and Li revealed the possible existence of more than one fluorescing states,[36] so the ns decay at short probe wavelengths can be confidently assigned as radiative emission from the excited-state non-H-bonded C102. The ps decay represents another depopulation channel. A similar biphasic decay has been observed by Barman et al. in their time-resolved fluorescence measurements of C102-phenol complexes,[37] and the faster decay has been interpreted as fluorescence quenching via internal conversion to a low-lying dark state (*e.g.*, a nonfluorescent charge transfer state) supported by TDDFT calculations.[25] However, no fluorescence quenching of C102 is experimentally observed in pure ethanol, and recent quantum chemistry calculations do not reveal any low-lying dark state in this case.[38]

Other possibilities for efficient depopulation on the ps timescale include non-radiative deactivation to the ground state and internal conversion to a nearby electronic state, *e.g.*, the first singly excited state of H-bonded C102. The latter pathway involves reformation of H-bond between C102 and nearby solvent molecules, and provides a straightforward explanation of the wavelength dependence of dynamics in transient absorption. If we were mainly probing the non-H-bonded C102 (reactant) at short wavelengths in transient absorption (see Fig. 1a) as evinced by its similar dynamics to the FSRS vibrational data (i.e., 1740 cm^{-1} mode in Fig. 3 insert), while having consistently larger contributions of H-bonded C102 (product) at longer probe wavelengths, the overall dynamics would become wavelength-dependent. In other words, the excited-state reactant population decay dominates at short probe wavelengths (*e.g.*, 630 nm) whereas the product population rise dominates at long probe wavelengths (*e.g.*, 725 nm). This mechanism is consistent with our transient absorption results (Table 1).

To examine the other possibility that the ps decay reflects non-radiative deactivation to the ground state, we perform the single-wavelength pump-probe measurement with λ_{pump} = λ_{probe} = 400 nm, wherein the recovery of ground state population after photoexcitation can be directly monitored. The time-resolved data trace exhibits a dominant 150 fs (59% amplitude weight, likely due to coherent effect that occurs within the cross correlation time of the optical setup)[28] and ~23 ps component (14% weight) in the recovery of ground-state bleaching signal (Fig. S4, ESI†), in addition to an even slower recovery on the ns timescale. However, the ps component may reflect excited-state dynamics that affect the overall signal as pointed out by Nibbering, et al.[39] Moreover, the 20–40 ps component has a large fitted amplitude weight in the overall ESA decay (*e.g.*, 53% at λ_{probe}=660 nm, Fig. 1a), and the interpretation of efficient non-radiative deactivation is inconsistent with the high fluorescence quantum yield (Φ_f ≈0.95) of C102 in ethanol.[40] Therefore, we attribute the observed ps decay in transient absorption data mainly to the aforementioned excited-state H-bond reformation.

Interestingly, the 1700 cm^{-1} band persists before decaying to noise level around 6 ps, yielding a time constant of ~3 ps (Fig. 3). Meanwhile, after the initial H-bond ruptures (blue τ_1<140 fs in Fig. 3), the 1740 cm^{-1} mode rises with a dominant ~12.6 ps time constant (blue τ_2 in Fig. 3). As a result, the 3 ps decay component of the 1700 cm^{-1} mode represents a poor match and suggests a different origin. Notably, the fast decay of Raman mode intensity may be due to a decrease of electric polarizability and/or loss of resonance enhancement as the vibronic wavepacket moves toward the equilibrium position at the bottom of the excited-state PES, rather than the population decrease. It is worth mentioning that a similar ~5 ps component was observed for C102 in aniline, another H-

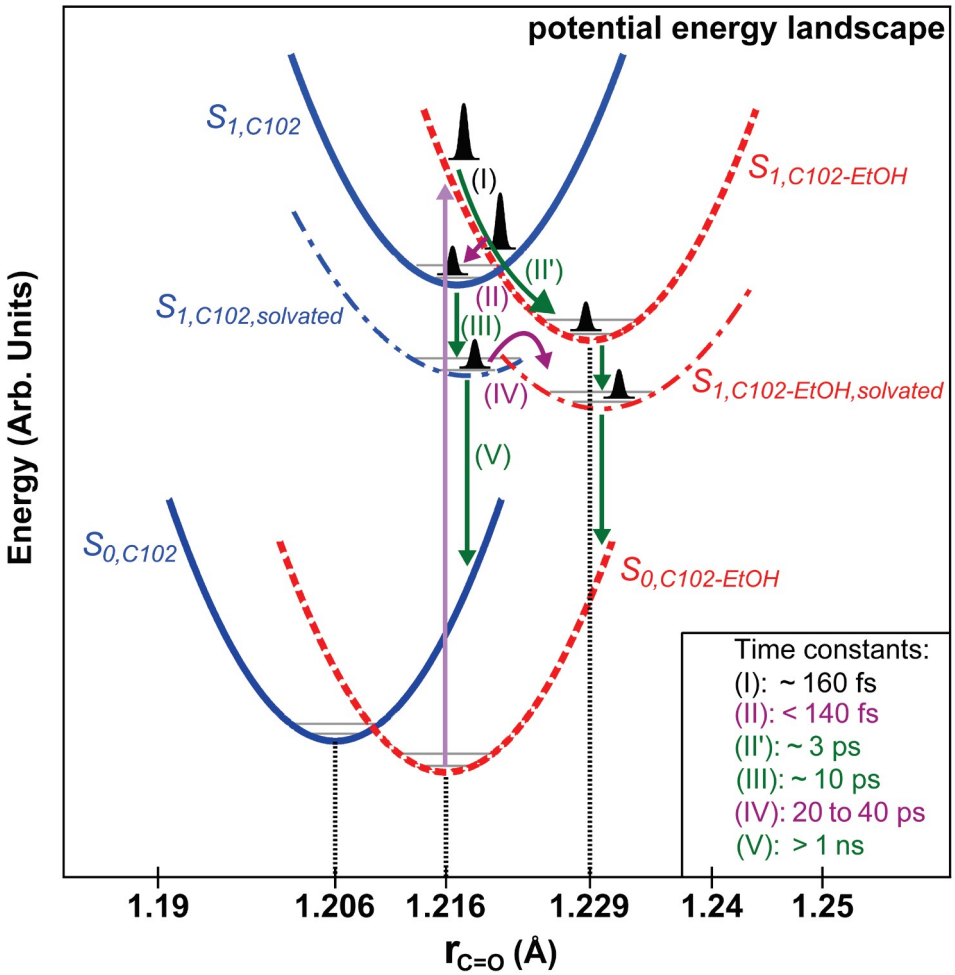

Fig. 4 Schematic of potential energy landscape of the electronic ground and excited states of C102 in ethanol solution. Blue solid and red dashed curves represent potential energy surfaces of free and H-bonded C102, respectively. Dash-dotted curves represent solvated electronic states. Following photoexcitation in the UV (magenta upward arrow), the evolution of excited-state wavepackets and population are indicated by downward green arrows with corresponding parenthesized Roman numerals (associated time constants are listed in the bottom right box). Purple arrows represent electronic state hopping (not vertical transition). The C=O bond lengths at equilibria (except for the two solvated singly excited states) are based on reported quantum chemistry calculation results.[38]

donating solvent, by Palit et al. using the optical pump/mid-IR probe technique.[23] We thus attribute the time constant of ~3 ps to vibrational relaxation within the same electronic state, which is largely facilitated by the attainment of an equilibrium geometry of the H-bonded C102-ethanol complex in S_1. Hence the observed mode intensity decay is likely a consequence of change of resonance conditions. Furthermore, the coexistence of 1700 and 1740 cm^{-1} after excited-state H-bond cleavage reveals that the cleavage is not the only reaction pathway, and a portion of excited-state population remains in the original electronic state instead of hopping onto the PES of non-H-bonded C102. In other words, our FSRS data unambiguously reveal the reaction pathway bifurcation of photoexcited C102 in ethanol, which has not been reported before.[41]

Regarding previous computational work,[7,8,25] we comment that the validity of predicting excited-state structural dynamics promptly after photoexcitation based on TDDFT calculations at equilibrium positions needs further improvement. In addition, the solvent effect was not explicitly taken into account in most calculations, whereas Xia et al. showed a non-negligible influence of solvent effect on the ground-state geometry and the electronic transition energy of C102 in H-donating solvents.[42] Therefore, it is advantageous for us to develop wavelength-tunable FSRS to address this long-standing discrepancy with a new perspective. We capture molecular structural snapshots after the excited state is populated by the fs photoexcitation pulse at 400 nm (see Experimental), but before relaxation to equilibrium either on the excited state or ground state via further energy dissipation pathways.[11,30] Above all, the excited-state PES is multidimensional in nature.

Minimal model of excited-state potential energy landscape

With the new data and current understanding of C102 in ethanol solution, we establish a "minimal" model (Fig. 4) that explains our experimental observations in the context of previous consensus by other groups.[18,19,29,35,37,38] The 400 nm photoexcitation pulse populates the first electronic excited

state of H-bonded C102 ($S_{1,\ C102\text{-}EtOH}$) and generates an excited-state wavepacket in the FC region. The wavepacket moves down the PES within ~160 fs (process I in Fig. 4, Δt_0 in Fig. 3) toward a region where electronic hopping onto another state, *e.g.*, the first excited state of non-H-bonded C102 ($S_{1,\ C102}$), can occur. The ultrafast hopping event (<140 fs, process II in Fig. 4, red τ_2 and blue τ_1 in Fig. 3) is accompanied by the cleavage of the H-bond between the C102 carbonyl oxygen and adjacent ethanol molecule, and is a barrierless process.[43,44] The newly generated exited-state non-H-bonded C102 is out of equilibrium with the surrounding solvent bath, and the initial solvation occurs on a timescale of ~10 ps (process III in Fig. 4, t_2 in Table 1 and blue τ_2 in Fig. 3) that matches the longitudinal relaxation time of ethanol by the dielectric continuum theory.[45] The observed 1740 cm^{-1} mode intensity increase is likely due to the resonance Raman effect because the new solvated, non-H-bonded C102 excited state ($S_{1,\ C102,\ solvated}$) is lower in energy (see Fig. 4) and its vibrational features are more enhanced with the 660 nm Raman pump. Subsequently, that excited state population either undergoes deactivation via radiative tranisition and returns to the electronic ground state on a ns timescale (process V in Fig. 4, t_4 in Table 1, and blue τ_4 in Fig. 3), or hops onto the solvated, H-bonded C102 excited state ($S_{1,\ C102\text{-}EtOH,\ solvated}$) within 20–40 ps (process IV in Fig. 4, t_3 in Table 1, and blue τ_3 in Fig. 3) during which the H-bond reforms between C102 and ethanol as favored in terms of equilibrium binding energy.[8,38] This mechanism is further corroborated by a previous report that two fluorescence peaks were observed for C102 in alcoholic solvents, and the 440/480 nm peak originates from the free/H-bonded C102 in the excited state[36] with the latter emission shows a delayed rise. This is likely due to the additional electronic transition step (IV) on the ps timescale as we propose in Fig. 4.

In addition, a portion of the originally generated excited-state population does not undergo electronic state hopping via H-bond clevage, but slides down the PES of $S_{1,\ C102\text{-}EtOH}$ and reaches the bottom well with ~3 ps time constant (process II' in Fig. 4, red τ_3 in Fig. 3), wherein radiative transition to the corresponding electronic ground state dominates the deactivation process. Notably, due to the small population of $S_{1,\ C102\text{-}EtOH}$ that bifurcates toward the bottom well and change in resonance Raman conditions in S_1,[28] the 1700 cm^{-1} mode dynamics cannot be tracked beyond ~6 ps despite the increase in excited-state population of H-bonded C102, hence the additional ns decay was not directly observed in this work.

Lastly, we note that our PES model is a minimal one because we do not include additional nearby electronic states that may or may not fluoresce, or include other dynamic pathways such as intersystem crossing and internal conversion to potentially contribute to some of the time constants we observe. However, our model depiction in Fig. 4 grasps the essence of both fs transient absorption (Fig. 1, Table 1, Fig. S3 and S4 in ESI†) and excited-state FSRS data (Fig. 2 and 3) and clearly reveals two critical photochemical reaction coordinates, i.e., the H-bond coordinate and the solvation coordinate on the fs to ps timescales, of photoexcited C102 in ethanol. It is notable that our model is also in accord with the estimate of equilibrium configurations and potential energies of electronic ground and excited states of both free C102 and C102-ethanol complex.[25,38] It is possible that the H-bond between C102 and ethanol is strengthened as predicted by calculations when the excited-state C102-ethanol complex relaxes to its equilibrium configuration, either along the original PES or via H-bond cleavage and subsequent reformation. However, it does not mean that the H-bond is strengthened at early stage upon excitation. Our comprehensive, microscopic view of the fate of a fluorophore in a H-bonding environment upon electronic excitation thus provides a firm structural dynamics basis to understand, engineer, and improve its optical properties.

Experimental

A detailed description of our newly built wavelength-tunable FSRS setup can be found in the ESI† (Fig. S1) and in our recent publications.[27,46] Briefly, an fs Ti:Sapphire laser amplifier system (Legend Elite USP-1K-HE, Coherent Inc.) generates ~35 fs, 4 W fundamental pulses (FP) at 800 nm center wavelength with 1 kHz repetition rate. About half of the FP is used to generate a wavelength-tunable narrowband Raman pump pulse (~2 ps, 510/660 nm for electronic ground/excited state measurement, ~10 mW average power that can be attenuated to ~2 mW for the actual excited-state measurement, ~200 µm focusing diameter), a broadband Raman probe (~60 fs, 520–580/670–760 nm for the electronic ground/excited state measurement to work in pair with the Raman pump on the Stokes side, ~150 µm focusing diameter), and an actinic pump (~30 fs, 400 nm, ~0.5 mW average power) used in our FSRS experiments.[41] The instrument response time is measured as the cross correlation between the fs actinic pump and Raman probe pulses in the 1-mm-thick solvent (*e.g.*, methanol, ethanol) sandwiched between two 500 µm quartz windows and is ~140 fs full width at half maximum.

Notably, the desired Raman probe tunability is achieved by implementing a laser sideband signal from the broadband up-converted multicolor array (BUMA), a technique recently developed in our laboratory.[47-49] One main reason to implement BUMA instead of the conventional way of generating supercontinuum white light using a thin sapphire plate[30,50] is that the photon counts to the red side of 660 nm are too low and also very close to the residual 800 nm fundamental pulse that cannot be completely filtered out. As a result, BUMA enables a suitable Stokes Raman spectral window to observe high-frequency vibrational modes with the 660 nm Raman pump pulse in the excited-state FSRS measurements. In particular, the free C102 in S_1 is pre-resonantly enhanced more than the H-bonded C102 so we observed clear dynamics of the 1740 cm^{-1} mode within the hundreds of ps detection time window. The 1700 cm^{-1} mode exhibits an ultrafast intensity drop due to loss of resonance enhancement as the vibronic wavepacket slides down the initial FC region (Fig. 3 and 4). The overall weak peak intensity of the C=O stretching modes in the excited state is due to the single chemical bond in response to the H-bonding change at the C102 carbonyl site, and the much reduced probe photon

counts in that region (even for BUMA generation) that affect the signal-to-noise ratio to some extent.

All the FSRS spectra on the Stokes side are presented as the stimulated Raman gain, i.e., [(Raman probe spectrum)$_{Raman\_pump\_on}$/(Raman probe spectrum)$_{Raman\_pump\_off}$ − 1].[31] The C102 fluorophore (Lambda Physik, standard laser dye) was used as received. All solvents including ethanol (Koptec) and C_2Cl_4 (J.T.Baker) are of reagent or higher grade, and were used without further purification. About 10 mM and 2 mM C102 solutions were used for electronic ground and excited state measurements, respectively. The high optical density of C102 in ethanol at 400 nm (~1/mm for 0.5 mM sample in UV/visible spectrum as shown in Fig. S2, ESI†) prevents us from using a solution of higher concentration than 2 mM in excited-state FSRS experiments (current OD≈3.8/mm at 400 nm). The FSRS setup can be turned into a standard transient absorption setup by blocking the Raman pump and tuning the broadband probe to the wavelength region of interest (*e.g.*, 625–725 nm, Fig. S3, ESI†) and reducing the concentration of C102 solution to 0.5 mM. All the experiments were performed at room temperature (22 °C) and ambient pressure (1 atm).

Quantum chemistry calculations of ground-state C102 have been performed in our lab to aid in vibrational mode assignment. Using density functional theory (DFT) with RB3LYP functional and the 6-31G+(d,p) basis set, the frequency and activity of ground-state Raman modes were calculated using Gaussian 09 software.[24] We calculated free C102 in ethanol, where the solvent effect was taken into account using the integral equation formalism based version of polarizable continuum method (IEF-PCM). The calculated frequencies are usually larger than the experimental values, and scaling factors of 0.96 to 0.99 are routinely used to make the frequency corrections.[51] In particular, the bands between ca. 1500 and 1650 cm^{-1} include several "ring modes", two strongest among which are peaked at ~1567 and 1634 cm^{-1} in excited-state Raman spectra in Fig. 2 (~1555 and 1599 cm^{-1} in the ground state). They can be correlated with the calculated modes at 1576 and 1618 cm^{-1}, respectively (scaling factor≈0.99). Both modes involve large-scale deformation of the chromophore phenyl and lactone rings while the C=O bond is largely at rest. The modes between 1100 and 1500 cm^{-1} mainly involve various ring/peripheral hydrogen motions that are not directly pertinent to H-bonding at the carbonyl site. The calculated C=O stretching mode is at 1712 cm^{-1}, where an asymmetric deformation of the lactone ring and a symmetric deformation of the phenyl ring are also involved. Thus, it is likely that this vibrational normal mode is not a true "local" mode isolated from the rest of the molecule.

Conclusions

In this study, our time-resolved FSRS experimental data analysis and modeling have revealed two important atomic coordinates for the excited-state structural dynamics of C102 in ethanol, i.e., the H-bonding coordinate and the solvation coordinate. Aided by wavelength-tunable FSRS, we confirm experimentally, for the first time, that the ultrafast H-bond cleavage induced by 400 nm photoexcitation occurs in the excited state S_1, rather than during excitation or after the FC dynamics. It is notable that the rate constants for H-bond cleavage and reformation are dramatically different, with the former being at least two orders of magnitude faster than the latter. These dynamics indicate that H-bond cleavage, which occurs ~160 fs following photoexcitation, is a barrierless process, whereas the H-bond reformation on a much longer timescale (>20 ps) involves surmounting a reaction barrier on the multidimensional excited-state PES of the fluorophore in solution. A reaction pathway bifurcation in the initially populated FC region has been identified with two characteristic time constants of ~140 fs and 3 ps. A unifying excited-state potential energy landscape involving free and H-bonded, solvated C102 in ethanol has been proposed with associated time constants for ultrafast electronic state hopping, vibrational relaxation, and radiative emission events.

Despite efforts and advances that have been made in this contribution, there are still important questions to be answered, *e.g.*, which low-frequency vibrational modes drive the H-bond breaking and formation dynamics,[5,11] how the conformational dynamics depend on different H-donating solvents, and what factors determine fine spectral splitting and shift of C=O bands in the excited state. We expect that these key points will be further elaborated with new advancement in computational chemistry focusing on the photoexcited state, as well as femtosecond vibrational spectroscopy with higher resolutions, both temporally and spectrally, over a wider spectral range and into more molecular dimensions. Plans of performing FSRS measurements on C102 in other H-bonding solvents and C102 derivatives in ethanol are currently ongoing in the lab to provide further comparison data. As a result, deeper structural dynamics insights of shape-responsive fluorophores and the governing structure-function relationship will truly enable the rational design and improvement of fluorescent molecules for a myriad of far-ranging applications from semiconductor industries (*e.g.*, photoacid, photoinduced electron transfer and/or proton transfer) to life sciences (*e.g.*, chemiluminescence, bioimaging, and biomedicine).

Acknowledgements

We thank Longteng Tang for help with figures and Breland Oscar for discussions. This work has been supported in part by the OSU Faculty Startup Grant, OSU General Research Fund, and the U.S. NSF CAREER Award (CHE-1455353) to C.F.

Notes and references

1 M. D. Joesten and L. J. Schaad, *Hydrogen Bonding*, Marcel Dekker, Inc., New York, NY, 1974.
2 G. A. Jeffrey and W. Saenger, *Hydrogen Bonding in Biological Structures*, Springer-Verlag, New York, NY, 1994.
3 E. T. J. Nibbering, H. Fidder and E. Pines, *Annu. Rev. Phys. Chem.*, 2005, **56**, 337-367.

4 R. M. Hochstrasser, *Proc. Natl. Acad. Sci. U.S.A.*, 2007, **104**, 14190-14196.
5 C. Fang, R. R. Frontiera, R. Tran and R. A. Mathies, *Nature*, 2009, **462**, 200-204.
6 C. J. Fecko, J. D. Eaves, J. J. Loparo, A. Tokmakoff and P. L. Geissler, *Science*, 2003, **301**, 1698-1702.
7 K.-L. Han and G.-J. Zhao, *Hydrogen Bonding and Transfer in the Excited State*, John Wiley & Sons, Ltd, The Atrium, Southern Gate, Chichester, West Sussex, UK, 2010.
8 G.-J. Zhao and K.-L. Han, *Acc. Chem. Res.*, 2012, **45**, 404-413.
9 P. Kukura, D. W. McCamant, S. Yoon, D. B. Wandschneider and R. A. Mathies, *Science*, 2005, **310**, 1006-1009.
10 G. S. Engel, T. R. Calhoun, E. L. Read, T.-K. Ahn, T. Mancal, Y.-C. Cheng, R. E. Blankenship and G. R. Fleming, *Nature*, 2007, **446**, 782-786.
11 B. G. Oscar, W. Liu, Y. Zhao, L. Tang, Y. Wang, R. E. Campbell and C. Fang, *Proc. Natl. Acad. Sci. U.S.A.*, 2014, **111**, 10191-10196.
12 R. J. D. Miller, *Science*, 2014, **343**, 1108-1116.
13 J. Zheng, K. Kwak, J. Asbury, X. Chen, I. R. Piletic and M. D. Fayer, *Science*, 2005, **309**, 1338-1343.
14 C. Fang, A. Senes, L. Cristian, W. F. DeGrado and R. M. Hochstrasser, *Proc. Natl. Acad. Sci. U.S.A.*, 2006, **103**, 16740-16745.
15 A. H. Zewail, *Femtochemistry: Ultrafast Dynamics of the Chemical Bond*, World Scientific, Singapore, 1994.
16 R. R. Frontiera, C. Fang, J. Dasgupta and R. A. Mathies, *Phys. Chem. Chem. Phys.*, 2012, **14**, 405-414.
17 E. T. J. Nibbering and T. Elsaesser, *Appl. Phys. B*, 2000, **71**, 439-441.
18 C. Chudoba, E. T. J. Nibbering and T. Elsaesser, *Phys. Rev. Lett.*, 1998, **81**, 3010-3013.
19 C. Chudoba, E. T. J. Nibbering and T. Elsaesser, *J. Phys. Chem. A*, 1999, **103**, 5625-5628.
20 C. D. Grant, K. E. Steege, M. R. Bunagan and E. W. Castner, *J. Phys. Chem. B*, 2005, **109**, 22273-22284.
21 B. Maity, A. Chatterjee and D. Seth, *Photochem. Photobiol.*, 2014, **90**, 734-746.
22 X.-M. Peng, G. L. V. Damu and C.-H. Zhou, *Curr. Pharm. Des.*, 2013, **19**, 3884-3930.
23 D. K. Palit, T. Zhang, S. Kumazaki and K. Yoshihara, *J. Phys. Chem. A*, 2003, **107**, 10798-10804.
24 M. J. Frisch, G. W. Trucks, H. B. Schlegel, G. E. Scuseria, M. A. Robb, J. R. Cheeseman, G. Scalmani, V. Barone, B. Mennucci, G. A. Petersson, et al., Gaussian 09, Revision B.1, Gaussian, Inc., Wallingford, CT, 2009.
25 G.-J. Zhao and K.-L. Han, *J. Phys. Chem. A*, 2007, **111**, 2469-2474.
26 W. Wang, W. Liu, I.-Y. Chang, L. A. Wills, L. N. Zakharov, S. W. Boettcher, P. H.-Y. Cheong, C. Fang and D. A. Keszler, *Proc. Natl. Acad. Sci. U.S.A.*, 2013, **110**, 18397-18401.
27 L. Zhu, W. Liu and C. Fang, *Appl. Phys. Lett.*, 2014, **105**, 041106.
28 L. Tang, W. Liu, Y. Wang, Y. Zhao, B. G. Oscar, R. E. Campbell and C. Fang, *Chem. Eur. J.*, 2015, **21**, 6481-6490.
29 F. Morlet-Savary, C. Ley, P. Jacques and J. P. Fouassier, *J. Phys. Chem. A*, 2001, **105**, 11026-11033.
30 F. Han, W. Liu and C. Fang, *Chem. Phys.*, 2013, **422**, 204-219.
31 W. Liu, F. Han, C. Smith and C. Fang, *J. Phys. Chem. B*, 2012, **116**, 10535-10550.
32 E. T. J. Nibbering, F. Tschirschwitz, C. Chudoba and T. Elsaesser, *J. Phys. Chem. A*, 2000, **104**, 4236-4246.
33 J. T. M. Kennis, D. S. Larsen, I. H. M. v. Stokkum, M. Vengris, J. J. v. Thor and R. v. Grondelle, *Proc. Natl. Acad. Sci. USA*, 2004, **101**, 17988-17993.
34 E. W. Castner, B. Bagchi, M. Maroncelli, S. P. Webb, A. J. Ruggiero and G. R. Fleming, *Ber. Bunsen-Ges. Phys. Chem.*, 1988, **92**, 363-372.
35 S. R. Inamdar, K. Chandrasekhar, D. C. Patil, N. N. Math and M. I. Savadatti, *Pramana - J. Phys.*, 1995, **45**, 279-290.
36 Y.-H. Liu and P. Li, *J. Lumin.*, 2011, **131**, 2116-2120.
37 N. Barman, D. Singha and K. Sahu, *J. Phys. Chem. A*, 2013, **117**, 3945-3953.
38 J. Su and D. Tian, *New J. Chem.*, 2014, **38**, 568-573.
39 F. Tschirschwitz and E. T. J. Nibbering, *Chem. Phys. Lett.*, 1999, **312**, 169-177.
40 G. Jones, W. R. Jackson, C. Y. Choi and W. R. Bergmark, *J. Phys. Chem.*, 1985, **89**, 294-300.
41 F. Han, *Ph.D. Thesis (Advisor: C. Fang)*, Department of Chemistry, Oregon State University, 2014.
42 W. Zhao, Y. Ding and Q. Xia, *J. Comput. Chem.*, 2011, **32**, 545-553.
43 X. Shi, P. Abbyad, X. Shu, K. Kallio, P. Kanchanawong, W. Childs, S. J. Remington and S. G. Boxer, *Biochemistry*, 2007, **46**, 12014-12025.
44 Y. Wang, L. Tang, W. Liu, Y. Zhao, B. G. Oscar, R. E. Campbell and C. Fang, *J. Phys. Chem. B*, 2015, **119**, 2204-2218.
45 J. L. McHale, *Molecular Spectroscopy*, Prentice-Hall, Upper Saddle River, NJ, 1999.
46 L. Zhu, W. Liu, Y. Wang and C. Fang, *Appl. Sci.*, 2015, **5**, 48-61.
47 W. Liu, L. Zhu, L. Wang and C. Fang, *Opt. Lett.*, 2013, **38**, 1772-1774.
48 L. Zhu, W. Liu and C. Fang, *Appl. Phys. Lett.*, 2013, **103**, 061110.
49 L. Zhu, W. Liu, L. Wang and C. Fang, *Laser Phys. Lett.*, 2014, **11**, 075301.
50 D. W. McCamant, P. Kukura, S. Yoon and R. A. Mathies, *Rev. Sci. Instrum.*, 2004, **75**, 4971-4980.
51 A. G. Baboul, L. A. Curtiss, P. C. Redfern and K. Raghavachari, *J. Chem. Phys.*, 1999, **110**, 7650-7657.

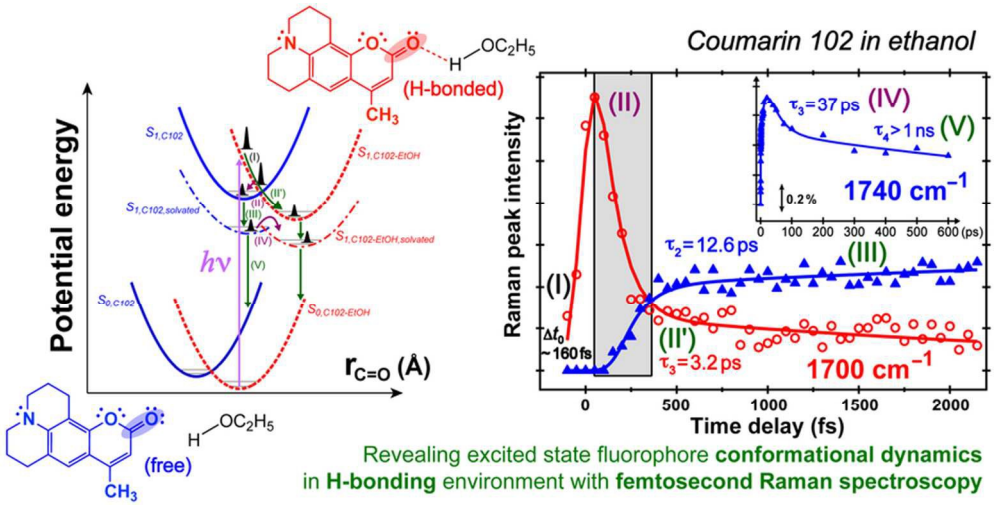

40x20mm (600 x 600 DPI)

Textual abstract (32 words)

The ultrafast hydrogen-bond breaking and reformation dynamics at the carbonyl site of Coumarin 102 dye molecule in ethanol is captured by femtosecond stimulated Raman Spectroscopy (FSRS) on the femtosecond to picosecond timescale.